Wide nonstoichiometry at 1000 °C of double perovskites $RBaFe_2O_{5+w}$

Antonin Cajka

Supervisor prof. Pavel Karen

KJM/3020 – Undergraduate Research II

Autumn 2014/Spring 2015

Description of the project aim

The project is divided into three main parts according to the progress of the lab work: synthesis of master samples, oxygen-content control, and analyses of samples. In the first part, two double-cell perovskites that differ somewhat in their low-temperature structure will be synthetized: $GdBaFe_2O_{5+w}$ and $PrBaFe_2O_{5+w}$. In addition, a perovskite isotypical with $PrBaFe_2O_{5+w}$ will be synthesized: $CeBaFe_2O_{5+w}$. In the second part, the nonstoichiometry parameter w in these samples will be varied by equilibrating under different pressures of oxygen at 1000 °C. The oxygen content and lattice parameters will be determined in the third part by respectively chemical analyses and powder X-ray diffraction.

Collected data for these three rare-earth based perovskites will expand our knowledge about this interesting type of mixed-valence compounds. The main goal of this study is to establish the limits of oxygen nonstoichiometry at temperatures around 1000 °C and to obtain dependences of this oxygen nonstoichiometry and of lattice parameters on temperature and oxygen pressure at high-temperature equilibrium.

Background for the project

Introduction

The *R*$BaFe_2O_5$ double-cell perovskites (where *R* is a trivalent rare-earth element) are interesting in that the iron atoms have oxidation states Fe^{2+} and Fe^{3+} in equal proportion [1]. These perovskites are mixed-valence compounds that show charge ordering at low temperatures and valence mixing at higher temperatures [2, 3]. Whereas at low temperatures there are separate Fe^{2+} and Fe^{3+} sites, increasing temperature makes one electron of Fe^{2+} to start hopping at the Fe^{3+} site and back, forming an $Fe^{2.5+}$ state [2]. This electron is the highest-energy valence electron of Fe^{2+}, the sole one with minority spin, and the hopping takes place between the two closest Fe sites that face each other. The result is an about 100 times higher electrical conductivity of the material [3, 4, 5]. The only way how this mixing electron can be shared between the two Fe atoms is that they have the same spin; the two iron atoms must be coupled ferromagnetically [3]. If in addition the entire phase is ferromagnetic, it becomes a source of spin-polarized current. This is interesting for spin transistors or magnetic RAMs. An important factor controlling the extent of the valence mixing is the oxygen nonstoichiometry *w* in *R*$BaFe_2O_{5+w}$. Increasing *w* removes Fe^{2+} needed to form the mixed-valence state $Fe^{2.5+}$ [6, 7]. Because the mixed-valence is the most interesting feature, non-stoichiometry data in these perovskites are available for values *w* close to zero, and less so for upper portion of the non-stoichiometry range.

Crystal structure of $RBaFe_2O_5$

The *R*$BaFe_2O_5$ oxides crystallize as double-cell perovskites with one oxygen site vacant [1]. The ideal high-temperature valence-mixed tetragonal structure is shown in the

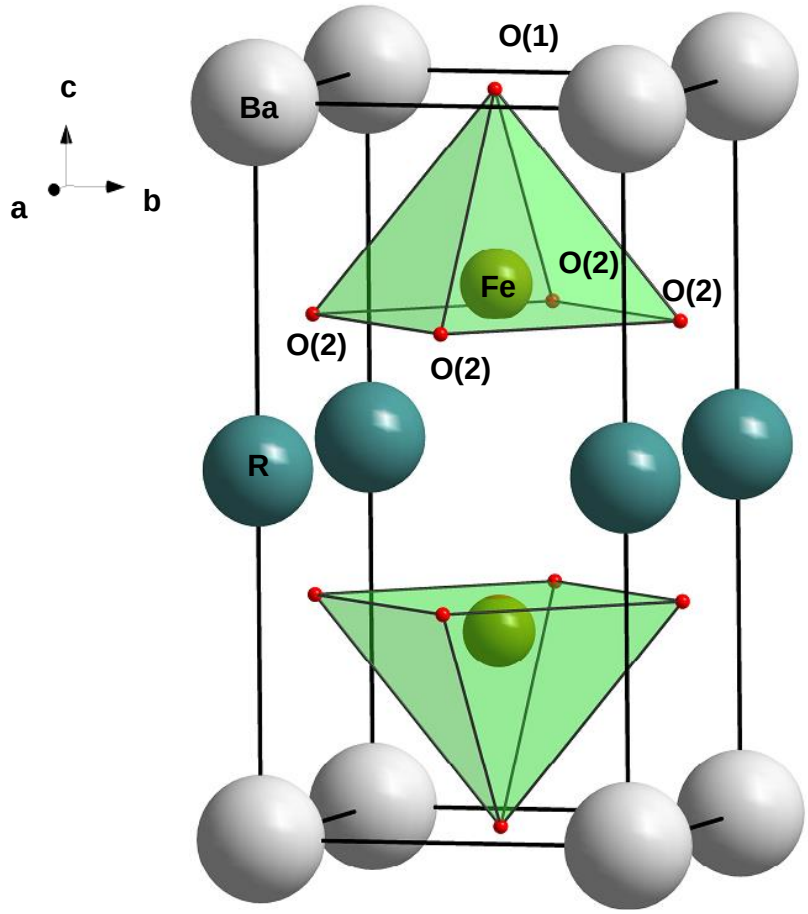

Figure 1. When the iron spins are magnetically ordered (at temperatures below the Néel temperature of about 440 K [8, 9]), the structure becomes slightly deformed orthorhombic due to magnetostriction [3]. The nonstoichiometry *w* is accommodated at the vacant site at ½ ½ ½. If this site were fully occupied by oxygen atoms, the composition of the double-cell perovskite would be RBaFe$_2$O$_6$.

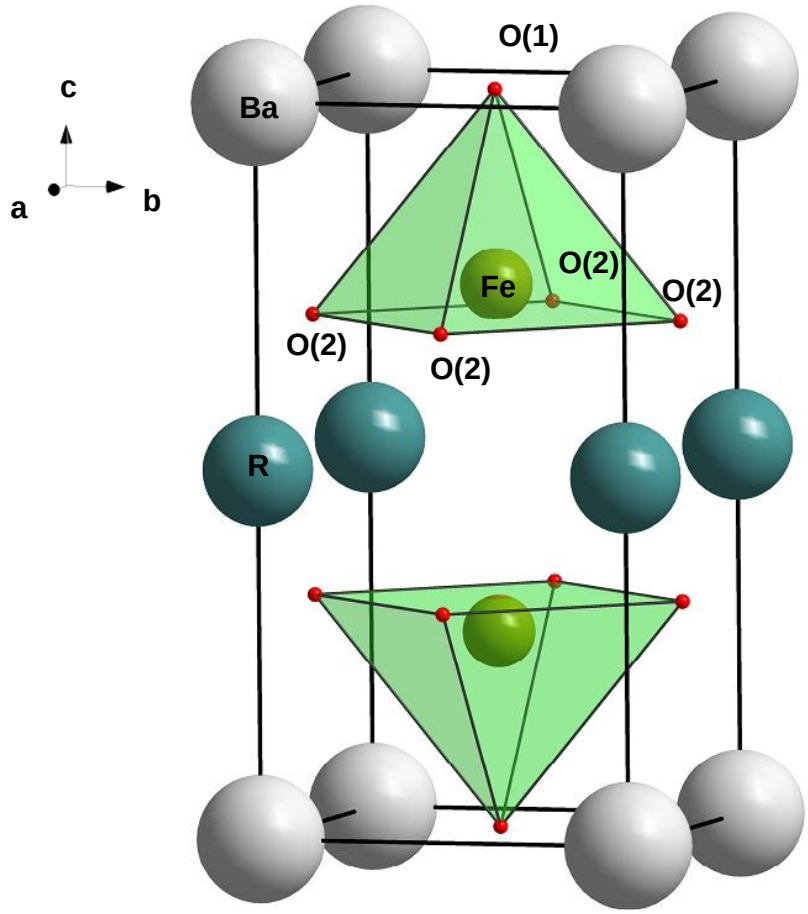

Figure 1 Unit cell of the high temperature valence mixed *R*BaFe$_2$O$_5$ phase with the ideal tetragonal *P/4mmm* symmetry [1].

Oxygen nonstoichiometry in RBaFe$_2$O$_{5+w}$

The extent of the oxygen nonstoichiometry in this structure increases with increasing size of the *R* atom. When *R* is small, the oxygen-nonstoichiometry range is narrow; the maximum allowed

value of the parameter *w* is low [10]. In the

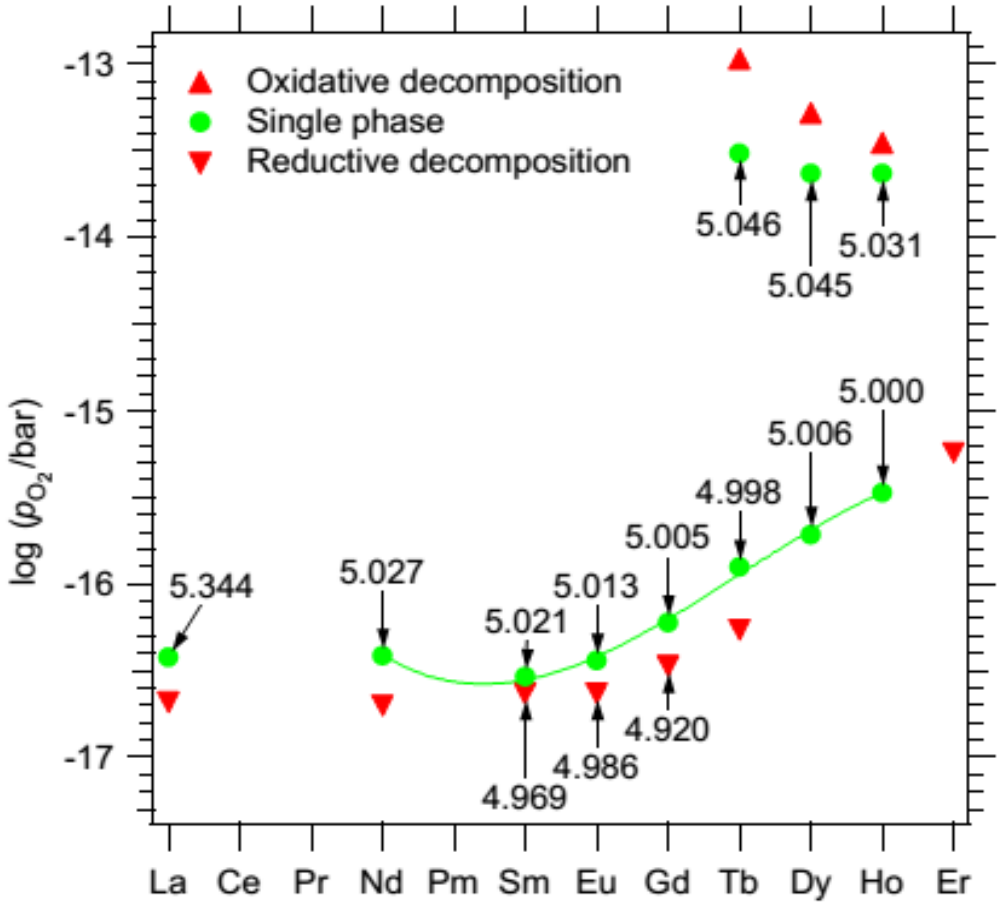

Figure **2**, limits of *w* upon oxidative and reductive decomposition are shown. We see that the Gd-based double perovskite is the first that doesn't decompose upon oxidation in atmosphere of pure oxygen at high temperatures [5]. Double perovskites with smaller rare-earth ions of *R* = Tb, Dy or Ho decompose under such conditions. As an example, when the partial pressure of oxygen is increased over the one with which $DyBaFe_2O_{5.045}$ is in equilibrium at 1000 °C, oxidative decomposition occurs into $DyFeO_3$ and $Ba_{1-y}Dy_yFeO_{3-w'}$ (y = 0.37 and w' = 0.44). Similarly, reductive decomposition occurs somewhere below oxygen content 5.006 per formula. A partially decomposed product was obtained at oxygen content 4.996. In an even more reducing atmosphere, a total oxygen content 4.888 was obtained for a mixture of a residual $DyBaFe_2O_5$, a $Ba(Dy,C)O_3$ perovskite, Dy_2O_3 and Fe. Similar behavior was seen also for Tb and Ho [3, 10].

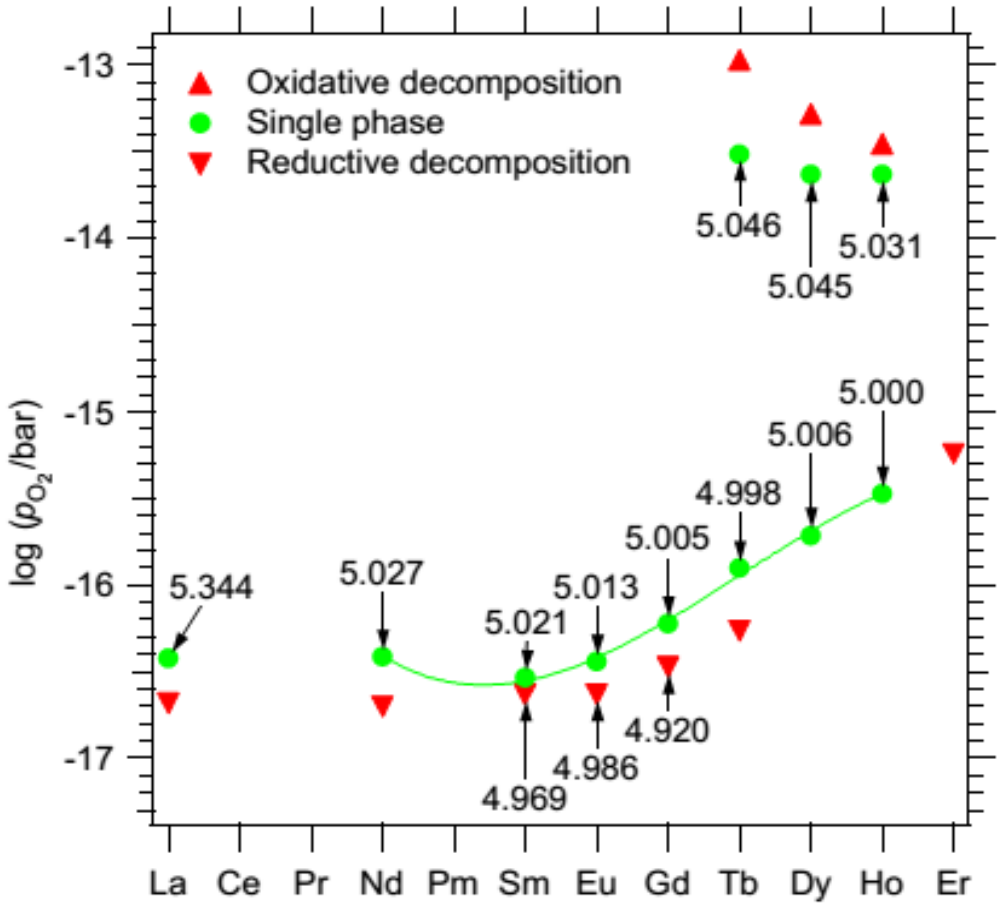

Figure 2 Limits in partial pressures of oxygen for formation of *R*$BaFe_2O_{5+w}$ at 1000 °C [10].

For Gd and rare-earth elements of higher atomic radius, only the reductive decomposition is observed. For example, the reductive decomposition of a sample with oxygen content lower than $NdBaFe_2O_{5.027}$ leads to a mixture of Fe, FeO, Fe_3O_4 and $Ba_{0.9}Nd_{0.1}FeO_{2.50}$ [1]. The nonstoichiometry range of the double perovskites with largest compatible rare-earth elements Pr and Ce (La does not form this phase) has not yet been established systematically. The same concerns the highest achievable value of *w* for several other *R* elements such as Gd. In this study, I will concentrate on these missing parameters completing the dataset for the temperature 1000 °C.

Descriptions of methods (experimental)

Chemicals, provenience, standardization and analysis

All chemicals and gases used in the study and their specifications, as well as its provenience are noted in the following list. Also the standardization and analysis conditions are specified for related compounds.

- Barium carbonate, $BaCO_3$ (<0.2 % Sr, reagent grade, Fluka). The starting material was a powder which was standardized by drying in a drying oven at 180 °C for 48 hours followed by cooling in a desiccator

- Cerium(III)nitrate hexahydrate, $Ce(NO_3)_3 \cdot 6H_2O$ (≥99.0 %, reagent grade, Fluka). The precise Ce content in cerium(III)nitrate hexahydrate was determined by gravimetric analysis: in three parallels, about 1 g of cerium(III)nitrate hexahydrate was precisely weighed into a porcelain crucible with a lid and annealed in the muffle furnace at 700 °C for 96 hours. The obtained CeO_2 was weighed and the amount of nitrate per mol of Ce was calculated

- Cerium(IV)sulfate solution, 0.1 M, Merck

- Citric acid monohydrate, $HOC(COOH)(CH_2COOH)_2 \cdot H_2O$, (reagent grade, <0.02 % sulfate ash, Fluka)

- Ferroin indicator solution, $[Fe(C_{12}H_8N_2)_3]SO_4$

- Gadolinium(III)oxide, Gd_2O_3 (99.99%, Stanford Materials). The Gd_2O_3 powder was standardized by annealing in a muffle furnace at 600 °C for 24 hours

- Hydrochloric acid, HCl (36.5 %, reagent grade, Merck)

- Iron (99.9 % purity, reagent grade, Riedel-de Haën). The starting material was a powder, and was standardized by sintering in a corundum boat in a flowing atmosphere of 10% H_2 in Ar4.6 at 650 °C for 5 hours

- Mohr's salt, $(NH_4)_2Fe(SO_4)_2.7H_2O$, (reagent grade, Merck)
- Nitric acid, HNO_3 (65%, reagent grade, Merck)
- Phosphoric acid, H_3PO_4 (85 %, reagent grade, Norsk Medisinal Depot)

- Praseodymium oxide, Pr_6O_{11} (99.99%, Metall Rare Earth Limited, Shenzhen, China). The Pr_6O_{11} powder was annealed in a flowing atmosphere of 9.59 % hydrogen for 68 hours to obtain green Pr_2O_3

- Silicon standard, Si (640d, Silicon Powder Line Position and Line Shape Standard for Powder Diffraction, NIST)

Gasses in 50 L pressure bottles

- Argon, Ar4.6 (99.996 % purity, AGA)
- Argon, Ar5.0 (99.999 %, ≤2 ppm O_2, AGA)
- Hydrogen (industrial quality, AGA)
- Hydrogen–argon mixture, 10 % H_2 (±2 %, AGA)
- Hydrogen–argon mixture, 9.59 % H_2 (±2 rel. %, special gas analyzed, AGA)
- Oxygen (industrial quality, AGA)

Methods used

Following methods were used to study the nonstoichiometry behavior of double cell perovskites $R\mathrm{BaFe_2O_{5+w}}$ with different *R* atoms (Gd, Pr and Ce):

- Liquid-mix synthesis of the master samples
- High temperature equilibration in a controlled atmosphere to obtain $R\mathrm{BaFe_2O_{5+w}}$
- Cerimetric titration to analyze the nonstoichiometry
- Powder X-ray diffraction to evaluate unit-cell parameters, or phase composition if needed

Syntheses of $RBaFe_2O_{5+w}$

Master samples of $R\mathrm{BaFe_2O_{5+w}}$ for *R* = Gd, Pr and Ce were synthetized from nanoscale precursor [7]. At first an organic amorphous precursor was obtained by liquid mixing of components as citrates in aqueous melted citric acid, yielding a viscous solution/melt that was subsequently dried and converted to an inorganic amorphous precursor by incineration in a covered crucible. The inorganic precursor was then calcined in order to remove all volatile components such as CO_2 and H_2O and convert the amorphous phase into a poorly crystalline double perovskite suitable for efficient sintering at temperatures around 1000 °C.

Citric acid was used as purchased. Prior use it was homogenized into individual crystals. As the rare-earth starting materials, powders of Gd_2O_3 and Pr_2O_3 and a water soluble cerium(III)nitrate hexahydrate were used. The oxide powder was dry mixed with the citric acid powder in a 3000 mL beaker, then some 50 ml of water was added on the glass bottom so that it was entirely wet, and the mixture was heated until the citric acid melted and the powder of the rare-earth oxide dissolved. Cerium(III)nitrate hexahydrate was added as aqueous solution. The reduction of nitrate ions was accompanied by evolution of NO_2, and the solution was heated and stirred until this brown gas ceased to evolve.

Placed in a covered 250 mL Erlenmeyer flask, the sintered iron bar was covered with distilled water and dissolved in a gradually added smallest necessary amount of 65% HNO_3, estimated as 10 mL 65**%** HNO_3 per 1 g of iron, while stirring the iron bar magnetically. Gas bubbles from reduction of the acid were observed during the dissolution process upon formation of red-colored transparent solution after all iron was completely dissolved. When a

small amount of black iron-oxide particles was formed, associated with passivation of the metal due to oxidation of the metal by the oxidizing acid, it was dissolved by a short heating the solution towards boiling point. The clear solution of the iron nitrate was then gradually added into the stirred citrate melt in the 3000 mL beaker so that the development of NO_2 was controlled. All nitrate ions were removed upon continued heating and stirring in the watch-glass covered beaker until the brown gas ceased to evolve. Then the beaker was let to cool down below 100 °C.

Standardized and powdered $BaCO_3$ was added to a cooled down solidified citrate melt in the beaker, to which about 100 ml of distilled water was added. Warming up was started again with mixing to dissolve all grains of $BaCO_3$ and obtain a homogeneous clear liquid.

Once a transparent orange-brown citrate melt with all metal ions was formed, it was poured into a porcelain bowl (diameter 30 cm) in the drying oven warmed up to 180 °C and let to decompose overnight into an organic based solid. This solid was hand crashed, homogenized with a porcelain pestle in the porcelain bowl, milled in the vibration mill for 1 hour and incinerated for 3 weeks in a covered porcelain crucible at 400 °C into the amorphous inorganic precursor.

$GdBaFe_2O_{5+w}$

The amount 12.9239 g of standardized Gd_2O_3 was dry mixed with 299.7 g of citric acid for 20 minutes. Iron bar of 7.96428 g was covered with 50 mL of distilled water and dissolved in a total of 80 ml of 65% HNO_3 after an intermittent formation of black iron oxide. The amorphous powder obtained from incineration was milled and calcined freely compacted in a corundum boat under conditions listed in Table 1. The calcinate was milled, pressed into cylindrical pellets of diameter 8 mm at uniaxial pressure 150 kg/cm^2 and sintered in a flowing atmosphere of Ar4.6 mixed with 10% H_2wetted in water at 18 °C. Specific conditions are listed in Table 1.

Table 1 Synthesis conditions of the $GdBaFe_2O_{5+w}$ master sample*

	***T* (°C)**	**Ar/H_2 ****	**log(*p*H_2O/bar)**	**log(*p*O_2/bar)**	***t* (hours)**
Calcination	900	151.5	-1.69	-15.15	25
Sintering	1000	19.7	-1.69	-15.17	25

* Specific oxygen contents according to the used partial pressure of oxygen in the synthesis.
** The ratio is by volume.

$PrBaFe_2O_{5+w}$

The amount 16.1935 g of Pr_2O_3 was dry mixed with 436.2 g of citric acid for 20 minutes. Iron bar of 11.59378 g covered with 45 ml of distilled water and dissolved in a total of 120 ml of 65% HNO_3. No problems with iron passivation occurred this time. The amorphous powder obtained from incineration was milled and then calcined under conditions listed in in Table 2. The calcinate was milled, pressed into pellets and sintered under conditions listed in Table 2.

Table 2 Synthesis conditions of the $PrBaFe_2O_{5+w}$ master sample

First	***T* (°C)**	**Ar/H_2**	**log(pH_2O/bar)**	**log(pO_2/bar)**	***t* (hours)**
Calcination	880	46.0(4)	-1.69	-16.58(1)	65
Sintering	1040	16.8(1)	-1.69	-14.69(1)	24

***Second* (not used)**	***T* (°C)**	**Ar/H_2**	**log(pH_2O/bar)**	**log(pO_2/bar)**	***t* (hours)**
Calcination	880	46.7(439)	-1.69	-16.56(8)	50
Sintering	1040	16.8(2)	-1.69	-14.69(0)	57

$CeBaFe_2O_{5+w}$

During the synthesis, 41.42495 g of cerium(III)nitrate hexahydrate was dissolved in 50 mL of destiled water in a 250 mL Erlenmeyer flask at room temperature upon manual stirring. On a hot plate, 408.6 g of citric acid was melted upon addition of 30 mL water.

Iron bar of 10.59380 g was covered with 45 ml of distilled water and dissolved in total of 110 ml of 65% HNO_3 after an intermittent formation of black iron oxide. Right before the iron solution, the cerium solution was added. Warm iron-nitrate solution was continuously added to the melted citric acid with cerium ions upon a vigorous reaction between these two leading to a complete removal of nitrate ions. After cooling down for 1 hour, 18.7832 g of barium carbonate and some 30 ml of distilled water were added and warming up to 150 °C was started. The calcinate was milled, pressed into pellets and sintered under conditions listed in Table 1.

Table 3 Synthesis conditions of the $CeBaFe_2O_{5+w}$ master sample

First	***T* (°C)**	**Ar/H_2**	**log(pH_2O/bar)**	**log(pO_2/bar)**	***t* (hours)**
Calcination	880	45.7(5)	-1.69	-16.55	68
Sintering	1020	16.8(3)	-1.68	-14.96(2)	26

***Second* (not used)**	***T* (°C)**	**Ar/H_2**	**log(pH_2O/bar)**	**log(pO_2/bar)**	***t* (hours)**
Calcination	880	31.4(229)	-1.60(6)	-16.91(56)	40
Sintering	1020	17.7(8)	-1.68	-14.93(4)	26

High-temperature equilibration

The oxygen nonstoichiometry in $RBaFe_2O_{5+w}$ was controlled by equilibration at 1000 °C in atmospheres containing an oxidative component, O_2, or a reductive component, H_2, both diluted to a various degree with the inert gas Ar to the concentration (expressed as the partial pressure of oxygen) that controls the desired value of the nostoichiometry parameter *w*. Three gas mixtures of H_2 were used: mixture of Ar4.6 and 10% H_2 mixture of Ar4.6 and 9.59% H_2, and likewise mixture of Ar4.6 and 100% H_2; to achieve the wide range of oxygen nonstochiometry

for either more or less reduced samples. Also equilibrations in pure 10% H_2 and 100% H_2 were tested to obtain the most reduced samples. All mixtures containing H_2 were wetted in water kept at controlled temperature of 18 °C. To obtain more oxidized samples, mixture of Ar4.6 and 100% O_2 in various ratios were used.

The sintered cylindrical pellet weighing 1 to 2 grams was hanged on a platinum wire inside a vertical tube furnace which was flushed with the gas for minimum 2 hours before the chamber was heated up. After 2 to 3 days of equilibration, the sample was quenched into a massive metal container inside the synthesis line, filled by high purity Ar5.0. The quenched sample was stored under argon in a glass vial having the volume of 2.5 mL.

Cerimetric titration

The cerimetric titration is a volumetric chemical analysis in which consumption of a Ce^{4+} solution of precise concentration is measured to fully oxidize a component of the analyzed sample. In our case, this component is Fe^{2+}:

$$Fe^{2+} + Ce^{4+} \leftrightarrow Fe^{3+} + Ce^{3+}$$

The content of Fe^{2+} is coupled with the oxygen content as follows: in the ideal case of $R$$BaFe_2O_5$ (w = 0), the oxidation state of iron is +2.5. This corresponds to the valence-mixed state of equally distributed Fe^{2+} and Fe^{3+} ions. In a sample with higher oxygen content, most of iron atoms have oxidation state 3+. In $R$$BaFe_2O_{5.5}$ (w = 0.5), the oxidation state of iron is exactly +3. Further increase in oxygen content creates Fe^{4+} ions in addition to Fe^{3+}. The hypothetical fully oxidized perovskite $R$$BaFe_2O_6$ would have an average oxidation state of +3.5, consisting of equal amounts of Fe^{3+} and Fe^{4+}. For any compositions that contain Fe^{4+}, a precisely weighed amount of Fe^{2+} in excess of present Fe^{4+} has to be added in the form of a standard compound $(NH_4)_2Fe(SO_4)_2.7H_2O$, Mohr's salt: The Fe^{4+} ions combine with the added Fe^{2+} into Fe^{3+}:

$$Fe^{4+} + Fe^{2+} \leftrightarrow 2Fe^{3+}$$

and the excess of Fe^{2+} is titrated.

Procedure

Quenched samples were crushed in an iron bowl, and milled with a pestle in an agate mortar to a fine powder. An exact amount of the powdered sample (from 0.12 g to 0.20 g) and also of the Mohr's salt (from 0.04 g to 0.1 g), when $w \geq 0.5$ was expected, were weighed into an ampule, some 5 mL distilled water was added, and the ampule was filled by Ar4.6 in order to keep the solution under an inert atmosphere. Then 5 mL of 36.5% HCl was added and the ampoule was sealed with a propane-butane burner. The dissolution of the sample was assisted by heating the bottom of the ampule with the sample. The solution had yellow color typical of iron. Also some transparent colorless crystals were usually observed on the bottom of the ampoule after cooling down. These crystals were dissolved immediately after the transfer to the Erlenmeyer flask used for titration.

After the ampoule cooled down, the dissolved sample was transferred into a 250 mL Erlenmeyer flask filled by Ar4.6, a small amount (20 to 30 mL) of 1:1 diluted 85% H_3PO_4 acid was added (to decompose the yellow iron complex), 2 drops of the purple ferroin indicator were added and also the walls of the flask were cleaned by splashing with some 10 ml of 36.5% HCl. The titration was performed in a 10 mL burette with the titration solution of Ce^{4+} ions. The indicator is a Fe^{2+}-1,1-phenantroline; an organic complex stabilizing Fe^{2+} oxidation state in its center. The indicator is not oxidized until all Fe^{2+} aqua-ions in the solution are oxidized. Above that point, the two or three drops of the Ce^{4+} solution oxidize the indicator which changes its color. Because of that, 0.04 mL were subtracted from the consumption for each titration. Each titration was performed in triplicate.

Powder X-ray Diffraction

Powder X-ray Diffraction (PXD) is a typical laboratory characterization technique to check purity and determine lattice parameters and phase composition of synthesized crystalline solids. The output is a diffractogram; collection of diffracted intensity profiles as a function of the angle of incident beam. In principle, the incident X-ray radiation beam of characteristic wave length diffracts on randomly oriented crystalline grains of a powder sample, while following the Bragg equation for constructive interference of the radiation beams diffracted from a set of atomic planes hkl:

$$2d_{hkl} \sin(\theta_{hkl}) = \lambda$$

There, λ is a wave length of the incident beam, θ_{hkl} is the angle of incidence, d_{hkl} is the spacing between planes.

Experimental set-up

In our experiment, the Bruker D8 X-ray diffractometer, with CuKα radiation (λ =1.5418 Å) source, in the Bragg–Brentano geometry (the angle of incidence equals the angle of detection), with the Lynxeye detector, 40 kV voltage and 40 mA current was used. In order to minimize oxidation, the powder sample was prepared right before the X-ray analysis by milling in an agate mortar from the sintered pieces stored under 4.6Ar. Small amount of the sample powder (~80 mg) was placed on an amorphous glass planar sample holder, mixed with a little amount of silicon standard (~5 mg), suspended in the drop of ethanol (to achieve homogenously flat distribution of the sample at the sample holder upon ethanol evaporation) and measured in the range of 10–100 ° in 2θ.

Rietveld refinement

For refinements of the obtained diffraction patterns, the GSAS program suite [11] was used. In the study, least squares fitting of the observed diffraction pattern with the calculated one were used. The goal of the refinement was obtaining of unit-cell parameters, besides confirming the

single-phase character of the double cell perovskite product. It is the precise refinement of unit-cell parameters that requires having an internal standard.

The silicon has space group *Fd-3m*, standard unit cell parameter *a* = 5.430825 Å and Si in general position ¼ ¼ ¼. The temperature factor for silicon was determined as 0.00185. Also the sharpness of the silicon peaks was refined and set up on the value 5.25. For some patterns these values were refined and changed. After the silicon sub-pattern was fitted, it was fixed and the double-cell perovskite phase was released for refinement (least-squares fit), including its fraction versus the standard silicon. The input values for this phase are listed in the **Table 4 *Pmmm* coordinates *x*, *y*, *z* and occupancies *occ* of the starting model for GSAS refinement of *R*$BaFe_2O_{5+w}$.**. The listed unit-cell parameters belong to the reported structures having *w* almost zero. These parameters were used as a template for additional refinements for close enough compositions. To refine compounds where *R* = Ce, same parameters as in the case of *R* = Pr were used. The diffraction peaks of the profile were fitted with the GSAS' pseudo-Voigt function #2 [12,13], which is a convolution of Gaussian and Lorentzian functions. A 8- or 9-coefficient Chebyshev polynomial function was used to fit the background. Temperature factor for each element was set up as 0.0085 and was refined. Finally, the unit-cell parameters were released and fitted.

Table 4 *Pmmm* coordinates *x*, *y*, *z* and occupancies *occ* of the starting model for GSAS refinement of *R*$BaFe_2O_{5+w}$.

	Starting unit-cell parameters (Å)							
a	3.9551				3.9650			
b*	3.9340				3.9665			
c	7.5919				7.6805			
	$GdBaFe_2O_{5.004}$ [7]				**$PrBaFe_2O_{5.001}$**** [14]			
Atom	***x***	***y***	***z***	***occ***	***x***	***y***	***z***	***occ***
R	0	0	½	1	0	0	½	1
Ba	0	0	0	1	0	0	0	1
Fe	½	½	0.2570	1	½	½	0.2651	1
O(1)	½	½	0	1	½	½	0	1
O(2)	½	0	0.3018	1	½	0	0.2998	1
O(3)	½	½	½	*w*	½	½	½	*w*

*in the case the *w* parameter is not close to the zero, the tetragonal unit cell has to be refined; having the space group *P4/mmm* and the *b* parameter equals to the *a* parameter

**same parameters were used in case of *R* = Ce

PXD characterization of the products

In order to check the products of incineration, calcination and sintering, the PXD was performed after each process. After incineration, an amorphous inorganic product was expected. After calcination, the single-phase but poorly crystalline product should be present, ideally with the perovskite structure (just disordered) and after the sintering, the ordered double-cell perovskite single-phase product should be observed.

The diffraction patterns for *R* = Gd, Pr and Ce after the incineration are shown in the Figure 3. The demonstrative comparison of products after the calcination and sintering is

shown for Ce in the Figure **Feil! Ugyldig selvreferanse for bokmerke.**. Based on the Figure 3 we can say all phases were amorphous after the incineration. We don't observe any peaks except of that belonging to the silicon standard used as the reference material in the compound containing cerium (in the blue line).

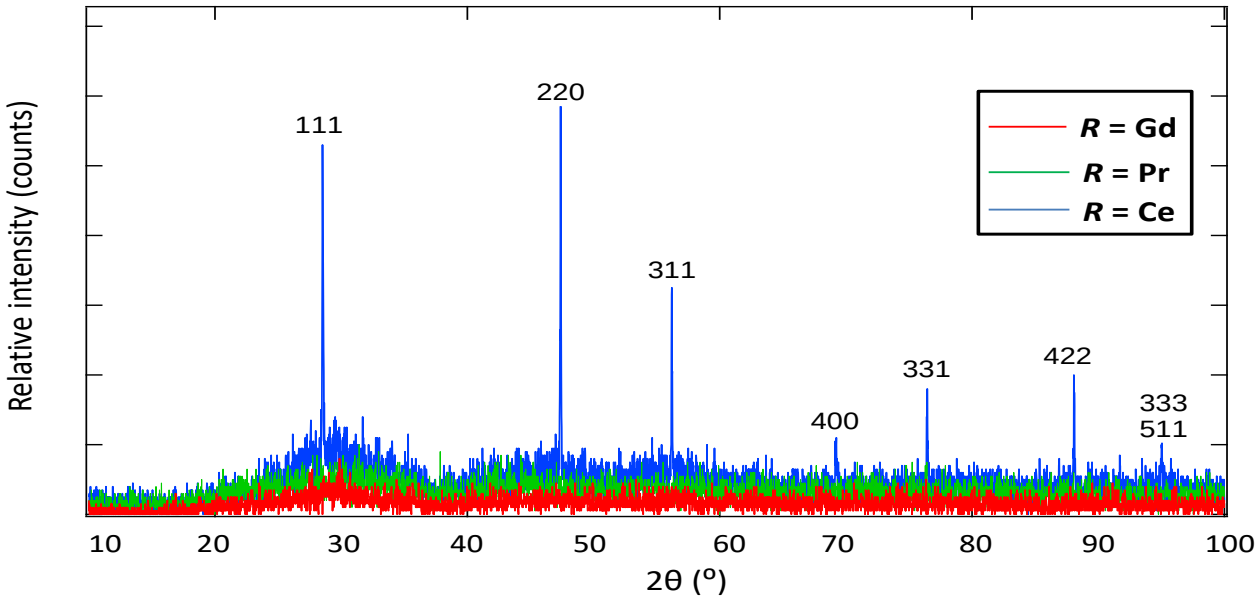

Figure 3 Diffraction patterns after the incineration step of the *R*$BaFe_2O_5$ synthesis.

In the Figure 4, two fitted diffraction patterns of compounds containing Ce are compared; after the sintering (a) and after the calcination (b). We observed some crystalline phases in both (in addition to the silicon phase). The phase after the sintering corresponds to the double-cell ordered perovskite structure $CeBaFe_2O_{5+w}$ (identified reflections in green). That confirmed us we successfully synthetized compound having the required structure.

The phase after the calcination was quite similar to the ordered phase. As the GSAS refinement confirmed, we observed a product consisted only of a cubic single-cell perovskite *Pm-3m* (reflections identified in blue). This product only needs to be ordered to achieve the double-cell perovskite structure.

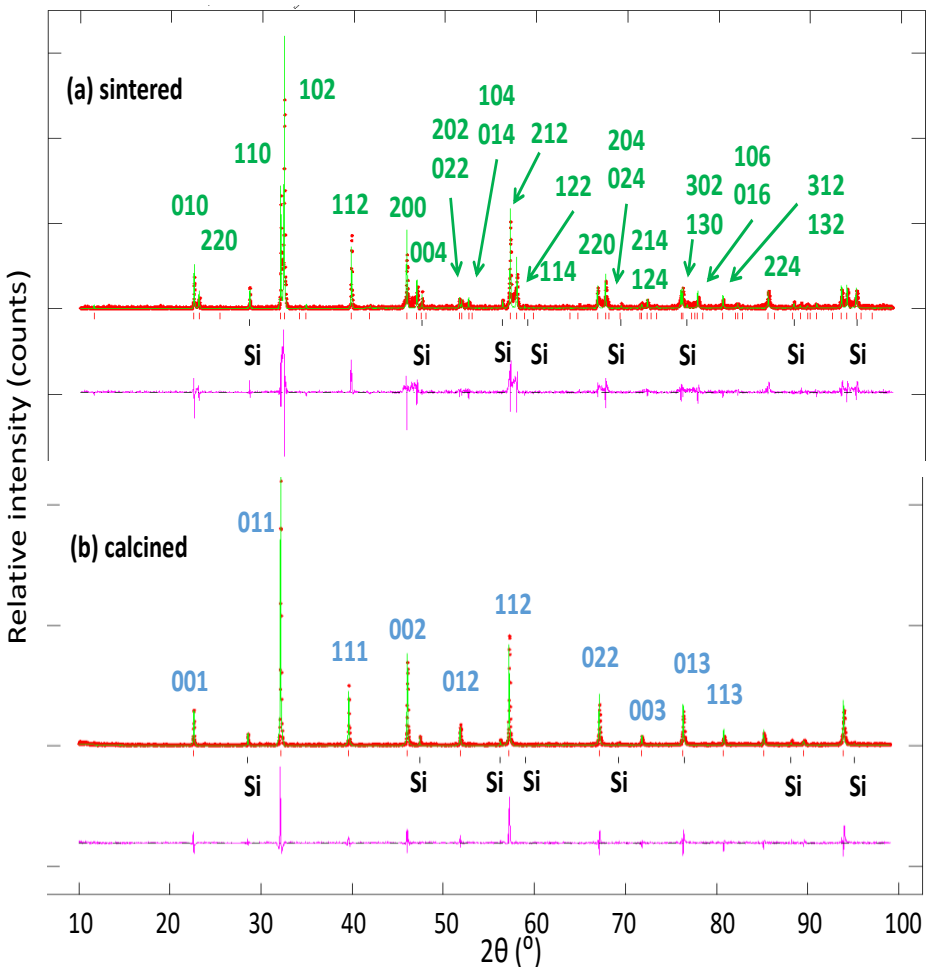

Figure 4 Diffraction patterns of $CeBaFe_2O_{5+w}$ after the calcination and sintering step of the synthesis. The *hkl* for *Pmmm* in blue, for *P4/mmm* in green. The observed pattern in red, fit in green,in magenta the difference. Si internal standard added. GSAS refinement to obtain unit-cell parameters.

In case of Gd and Pr, obtaining of the double-cell perovskite structure was also confirmed after the sintering. After the calcination, always the multiphase product consisting of a cubic single-cell perovskite, a small amount of ordered double-cell perovskite and also of some impurities was observed. Those samples were less crystalline. Because of that, the peaks were slightly broader than in the case after the sintering.

The high temperature equilibration and the oxygen content analysis

The oxygen content was determined by the cerimetric titration as introduced previously. The results for each *R* in $RBaFe_2O_{5+w}$ follow. For Gd, the overviewing values were collected. For Pr, the very detailed study was performed. In case of Ce, only 4 points were collected; in order to get a basic understanding about the compound (included in the Pr chapter).

$GdBaFe_2O_{5+w}$

Obtained results and the equilibration conditions are listed in the Table 5. In the

As is noticeable from the Table 5, the highest achievable value of w = 564 gave us the equilibration in the pure O_2. No oxidative decomposition was observed - the sample was non-magnetic, having the double-cell perovskite structure. The lowest value we got was after the equilibration in the mixture of Ar4.6 and 10% H_2 (volume ratio 9.0). The nonstoichiomety parameter w equaled to 0.005. Also no reductive decomposition was observed. It confirmed us our expectation based on the ref [1]: this double-cell perovskite structure is stable in a wide range of oxygen nonstoichiometry.

From the Figure 5 we can see how the parameter w varies with the different partial pressures of oxygen. The small variation in the partial pressure, especially for the lower values within the interval −15.80 to −9.94 causes a big difference in w. This lasts up to the achieving the w value 0.5. In this point, all Fe^{2+} becomes theoretically oxidized to Fe^{3+} and the valence mixed state doesn't occur any longer. For higher partial pressures of oxygen beginning by the point $\log(pO_2)$ = −8.00 only the small variations in the w parameter were observed; w reminds slightly above the value 0.5 in the wide range of partial pressures. It says us the highest possible oxygen occupancy was almost achieved, and also the oxidation up to Fe^{4+} state isn't as favorable as the oxidation of Fe^{2+} (even for the highest partial pressures).

The lowest achievable limits seemed to be close to the value w = 0, having almost the same amount of Fe^{3+} and Fe^{2+} ions. These limits weren't approved in our study. The sample having the w value 0.384 under the $\log(pO_2)$ = −12.30 wasn't included into our consideration. The higher oxygen content was caused by a sample oxidation before the analysis.

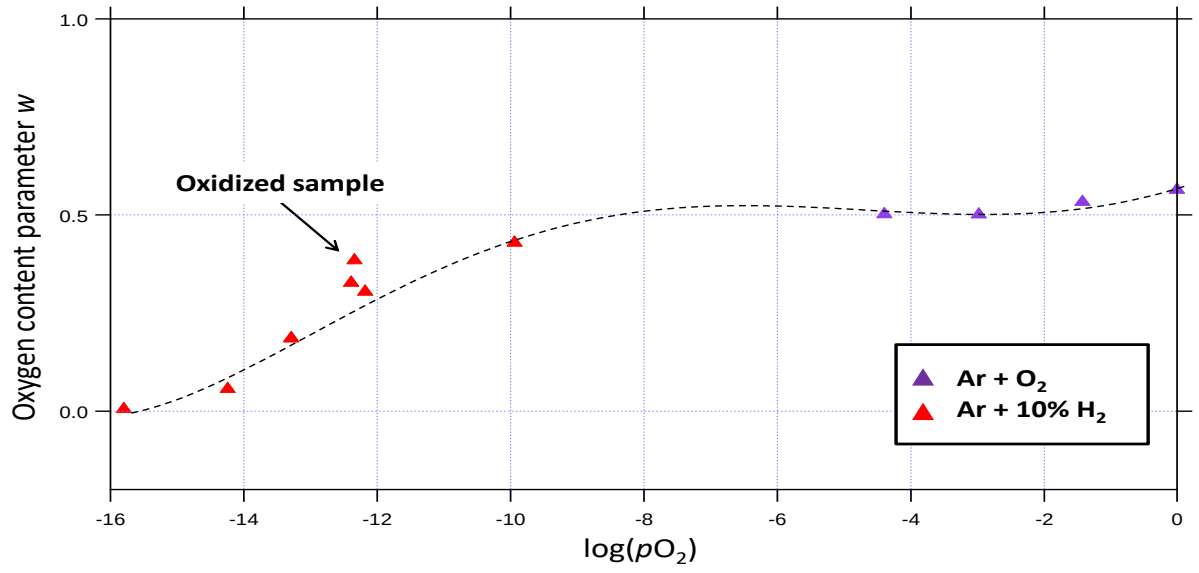

Figure 5

Table 5 Equilibration conditions of the nonstoichiometry control in $GdBaFe_2O_{5+w}$ at 1000 °C

5+*w*	Ar/H_2	Ar/O_2	log(pH_2O/bar)	log(pO_2/bar)	*t* (hours)
5.005(1)	9.0(0)	-	−1.69	−15.80(1)	45
5.056(3)	61.6(0)	-	−1.71	−14.24(1)	69
5.185(3)	181(8)	-	−1.71	−13.29(4)	66
5.304(1)	613(14)	-	−1.70	−12.18(2)	28
5.327(1)	500(36)	-	−1.71	−12.39(6)	49
5.429(3)	4654(264)	-	−1.71	−9.94(10)	69
5.501(5)	-	973(54)	−1.71	−2.98(2)	68
5.502(1)	-	Ar	−1.70	−4.40(0)	48
5.533(3)	-	25.2(2)	−1.71	−1.43(3)	69
5.564(3)	-	O_2	−1.71	−0.01	96

As is noticeable from the Table 5, the highest achievable value of *w* = 564 gave us the equilibration in the pure O_2. No oxidative decomposition was observed - the sample was non-magnetic, having the double-cell perovskite structure. The lowest value we got was after the equilibration in the mixture of Ar4.6 and 10% H_2 (volume ratio 9.0). The nonstoichiomety parameter *w* equaled to 0.005. Also no reductive decomposition was observed. It confirmed us our expectation based on the ref [1]: this double-cell perovskite structure is stable in a wide range of oxygen nonstoichiometry.

From the Figure 5 we can see how the parameter *w* varies with the different partial pressures of oxygen. The small variation in the partial pressure, especially for the lower values within the interval −15.80 to −9.94 causes a big difference in *w.* This lasts up to the achieving the *w* value 0.5. In this point, all Fe^{2+} becomes theoretically oxidized to Fe^{3+} and the valence mixed state doesn't occur any longer. For higher partial pressures of oxygen beginning by the point log(pO_2) = −8.00 only the small variations in the *w* parameter were observed; *w* reminds slightly above the value 0.5 in the wide range of partial pressures. It says us the highest possible oxygen occupancy was almost achieved, and also the oxidation up to Fe^{4+} state isn't as favorable as the oxidation of Fe^{2+} (even for the highest partial pressures).

The lowest achievable limits seemed to be close to the value *w* = 0, having almost the same amount of Fe^{3+} and Fe^{2+} ions. These limits weren't approved in our study. The sample having the *w* value 0.384 under the log(pO_2) = −12.30 wasn't included into our consideration. The higher oxygen content was caused by a sample oxidation before the analysis.

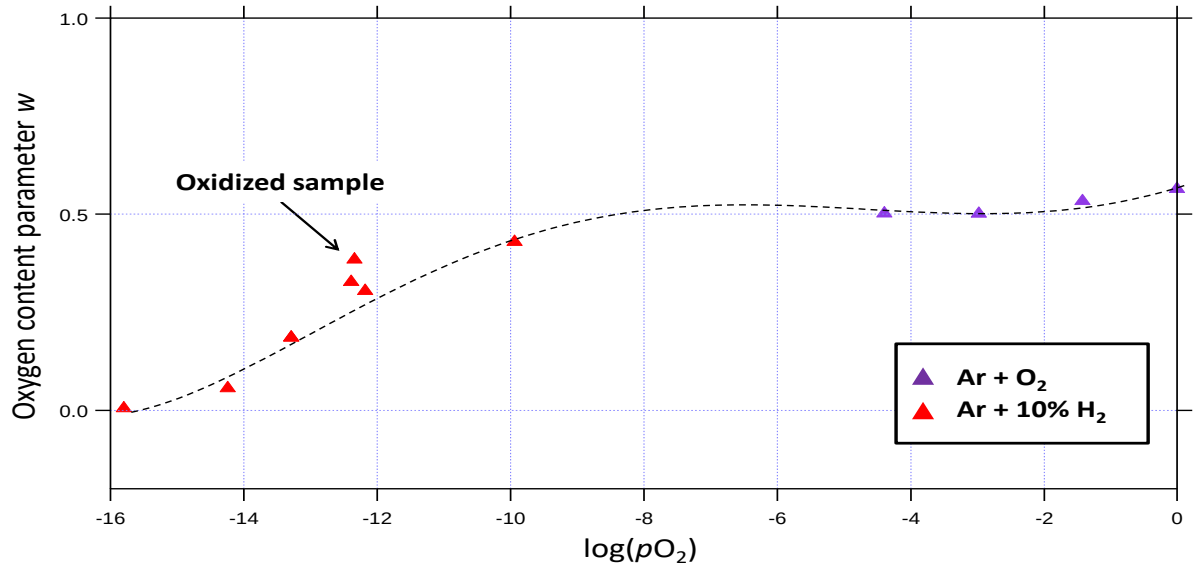

Figure 5 Oxygen content parameter *w* over log(pO_2) dependence for $GdBaFe_2O_{5+w}$ in two gas-mixtures

$PrBaFe_2O_{5+w}$ and $CeBaFe_2O_{5+w}$

The study over the wide range of the oxygen nonstoichiometry was performed in case of Pr. For the Ce compound the basic overview follows. Obtained results and the equilibration conditions are listed in the Table 5 (for *R* = Pr) and Table 7 (for *R* = Ce). The graphical representation of the oxygen content parameter *w* dependence over log(pO_2) is in the Figure 6 (for both).

Table 6 Equilibration conditions of the nonstoichiometry control in $PrBaFe_2O_{5+w}$ at 1000 °C

5+*w*	Ar/H_2	Ar/O_2	log(pH_2O/bar)	log(pO_2/bar)	*t* (hours)
4.991(4)	3.41(56)	-	−1.71	−16.56(11)	49
5.067(3)	9.97(18)	-	−1.71	−16.45(4)	46
5.070(2)	5.52(19)	-	−1.71	−16.22(3)	67
5.084(5)	4.82(5)	-	−1.71	−16.32(1)	48
5.088(4)	9.0(0)	-	−1.71	−15.84(0)	71
5.128(1)	9.0(0)	-	−1.71	−15.83(0)	100
5.134(3)	9.0(0)	-	−1.71	−15.83(0)	54
5.148(5)	10.15(81)	-	−1.71	−15.74(6)	52
5.195(2)	15.7(11)	-	−1.71	−15.40(6)	69
5.263(4)	31.6(7)	-	−1.71	−14.82(2)	70
5.357(2)	63.2(62)	-	−1.71	−14.23(8)	67
5.365(3)	61.6(0)	-	−1.71	−14.24(0)	69

5.391(1)	182(5)	-	−1.71	−13.30(3)	66
5.437(1)	557(11)	-	−1.71	−12.30(2)	69
5.452(2)	530(0)	-	−1.71	−12.34(0)	73
5.484(1)	6332(95)	-	−1.71	−9.34(4)	73
5.511(9)	-	Ar	−1.71	−4.40(0)	96
5.538(3)	-	1214(246)	−1.71	−3.06(9)	72
5.631(1)	-	39(6)	−1.71	−1.60(6)	66
5.818(5)	-	O_2	−1.71	−0.01	60

In the case of larger Pr atoms in the structure, also no oxidative decomposition was observed even after the equilibration in the pure O_2, as in the case of Gd. Instead, the nonstoichiometry parameter achieved the highest value 0.818. The lowest achieved value without observing the reductive decomposition gave us the equilibration in the mixture of pure H_2 and Ar4.6. After that, we observed the negative value w = −0.009, while log(pO_2) = −16.56. For log(pO_2) = −16.75, the reductive decomposition was observed. The equilibrated sample shown the magnetic properties pointing out a partly decomposed double-cell perovskite structure; and some iron components presented in addition.

Table 7 Equilibration conditions of the nonstoichiometry control in $CeBaFe_2O_{5+w}$ at 1000 °C

5+*w*	**Ar/H_2**	**Ar/O_2**	**log(pH_2O/bar)**	**log(pO_2/bar)**	***t*** **(hours)**
5.499(6)	511(33)	-	−1.71	−12.38(8)	47
5.534(28)	4614(207)	-	−1.71	−9.96(7)	45
5.546(26)	-	Ar	−1.71	−4.40(0)	90
5.624(28)	-	O_2	−1.71	−0.01(0)	42

The double-cell perovskite samples containing cerium were equilibrated only in the higher partial pressures of oxygen. We found out the highest achievable value of w is 0.624; after the equilibration in pure O_2. No oxidative decomposition was observed.

Based on the Figure 6, we can see the similar tendency in the variation of w parameter as in the Gd case for both Pr and Ce. In the interval between −12.34 and −4.40 there is a gap where the w remains approximately 0.5. Consequently, with further increase in log(pO_2) we observed increase in the *w;* for Pr this increase is significant. This last up to the reaching of the highest values performed in pure O_2. For Pr, we observed also the huge increasing of w within the interval of the lowest pressures; approximately up to the value log(pO_2) = −12.34. Within the both, either the interval of the lowest or the highest pressure it is noticeable that the slight difference in the oxygen pressure causes the significant difference in the w parameter.

For Ce, those changes in log(pO_2) are not so significant. The oxygen content varies slightly above the value 0.5. Only after the equilibration in the pure O_2 the w value achieved the higher oxygen content 0.624.

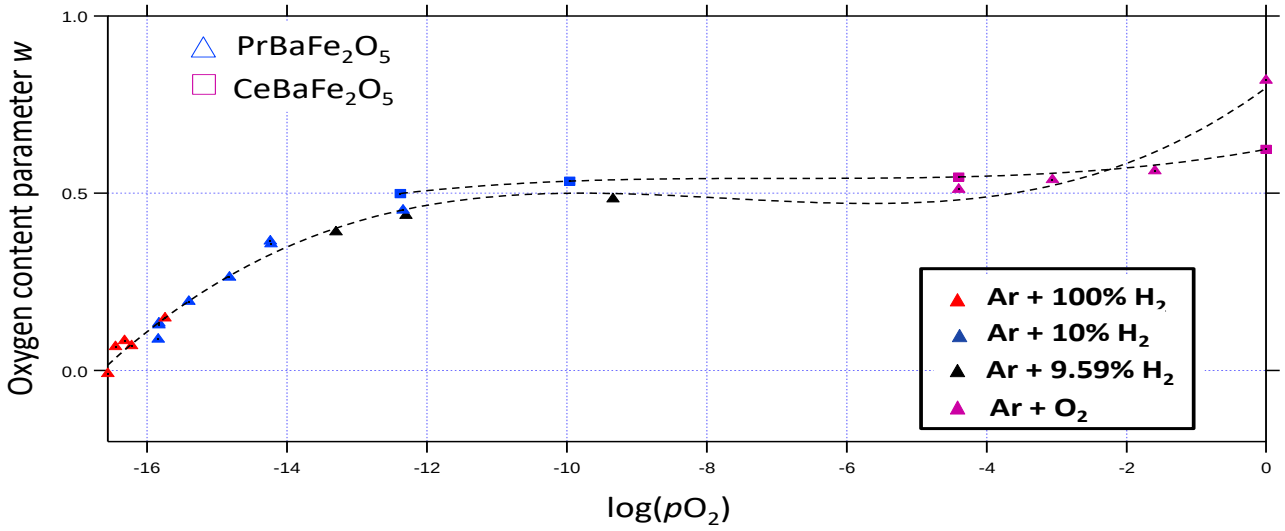

Figure 6 Oxygen content parameter *w* over log(pO_2) dependence for $PrBaFe_2O_{5+w}$ and $CeBaFe_2O_{5+w}$

Unit-cell parameters refinement

Unit cell parameters were refined for representative samples. Also the unit cell volume was determined. The results are shown in the Table 8 (for *R* = Gd),Table 9 (for *R* = Pr) and Table 10 (for *R* = Ce) . The graphical representation of the plotted dataset is shown in the Figure 7.

Table 8 The unit cell parameters control for $GdBaFe_2O_{5+w}$

$GdBaFe_2O_{5+w}$	Refined unit-cell parameters			Unit cell volume
Oxygen content parameter 5+*w*	*a* (Å)	*b* (Å)	*c* (Å)	*V* (Å^3)
5.005(1)	3. 9525(1)	3.9325(1)	7.5907(2)	117.986(5)
5.056(3)	3.9489(1)	3.9359(1)	7.6037(2)	118.181(5)
5.185(3)	3.9396(1)	-	7.6351(3)	118.500(5)
5.304(1)	3.9364(1)	-	7.6719(3)	118.875(5)
5.327(1)	3.9376(1)	-	7.6676(3)	118.890(6)
5.429(3)	3.9301(1)	-	7.7188(3)	119.225(9)
5.501(5)	3.9386(1)	-	7.8103(2)	121.159(8)
5.502(1)	3.9331(2)	-	7.8241(4)	121.036(2)
5.533(3)	3.9373(1)	-	7.8126(2)	121.114(6)
5.564(3)	3.9341(1)	-	7.8140(2)	120.940(6)

According to our expectations, the orthorhombic phase $GdBaFe_2O_{5.005}$, having the lowest oxygen content parameter *w* has also the smallest unit-cell (*V* = 117.986 Å^3). By crossing the value approximately *w* = 0.10 (as suggested in the Figure 9), the phase becomes tetragonal and starts to grow in the *c*-direction, while shortens in the *a*-direction. It is due to the accommodation of additional oxygen in the middle vacant ½ ½ ½ position. Also the unit-cell volume increases. This trend is observed until the *w* parameter crosses the value approximately 0.5. Suddenly, a big increase in the *c*-parameter and also *a*-parameter occurs (almost 0.5 Å difference according to the expected values for the *c*-parameter and 0.05 Å for the *a*-parameter). After the big jump, the oxygen content parameter *w* achieves the value 0.501 and the unit-cell volume reaches its highest value 121.159 Å^3. Further, the unit-cell parameters don't change magnificently; mainly keep the previously introduced trend until the *w* achieves its maximal value 0.564, it lowers the unit-cell volume slightly.

Table 9 The unit cell parameters control for $PrBaFe_2O_{5+w}$

$PrBaFe_2O_{5+w}$	Refined unit-cell parameters			Unit cell volume
Oxygen content parameter 5+*w*	*a* (Å)	*b* (Å)	*c* (Å)	*V* (Å^3)
4.991(4)	3.9744(2)	3.9664(2)	7.6793(3)	121.058(6)
5.067(3)	3.9705(1)	-	7.6780(2)	121.045(8)
5.070(2)	3.9680(1)	-	7.6825(3)	120.987(1)
5.084(5)	3.9694 (1)	-	7.6785(1)	120.990(4)
5.088(4)	3.9661(10)	-	7.6904(1)	120.989(8)
5.128(1) **missing**		-		
5.134(3)	3.9680(1)	-	7.6923(1)	121.114(6)
5.148(5)	3.9672(8)	-	7.6924(1)	121.069(6)
5.195(2)	3.9631(8)	-	7.7101(2)	121.098(6)
5.263(4)	3.9639(8)	-	7.7335(2)	121.513(6)
5.357(2)	3.9604(9)	-	7.7507(2)	121.566(7)
5.365(3)	3.9610(6)	-	7.7470(1)	121.548(2)
5.391(1)	3.9585(7)	-	7.7607(2)	121.608(6)
5.437(1)	3.9566(6)	-	7.7698(2)	121.632(5)
5.452(2)	3.9564(6)	-	7.7738(2)	121.682(5)
5.484(1)	3.9543(7)	-	7.7847(2)	121.683(1)
5.511(9)	3.9539(7)	-	7.7896(1)	121.778(5)
5.538(3)	3.9526(7)	-	7.7903(2)	121.708(6)
5.631(1)	3.9513(1)	-	7.7922(2)	121.654(6)
5.818(5)	3.9427(8)	-	7.7930(8)	121.139(6)

In case of Pr, the smallest obtained unit-cell corresponds surprisingly to the tetragonal phase $PrBaFe_2O_{5.070}$ having the volume of 120.987 Å^3. However, due to the very small deviation in the unit cell volume, also the tetragonal phases $PrBaFe_2O_{5.067}$, $PrBaFe_2O_{5.084}$ and $PrBaFe_2O_{5.088}$ can be considered the smallest. The phase $PrBaFe_2O_{5.991}$ having the lowest oxygen content

should also belong to the group of smallest, but due to the orthorhombic distortion gained a higher volume. The phase $PrBaFe_2O_{5.067}$ having the second lowest oxygen content was already considered tetragonal. The variation of unit-cell parameters is quite similar as in the previous case of Gd. The *c*-parameter increases while the *a*-parameter decreases with increasing *w*; until w achieves its maximal value 0.818. After that, it lowers its unit-cell volume again.

Table 10 The unit cell parameters control for $CeBaFe_2O_{5+w}$

$CeBaFe_2O_{5+w}$	Refined unit-cell parameters			Unit cell volume
Oxygen content parameter 5+*w*	*a* (Å)	*b* (Å)	*c* (Å)	*V* (Å^3)
5.499(6)	3.9735(1)	-	7.7464(3)	122.305(5)
5.534(28) **missing**				
5.546(26) **missing**				
5.624(28) **missing**				

By X-ray measurement, we detected partly decomposed compounds after the equilibration in the higher pressures of oxygen. However, the double cell-perovskite compound was the dominant phase in the case of the lowest oxygen pressure. Because of that, the refinement was done; in order to demonstrate the unit-cell size of $CeBaFe_2O_{5.499}$. It shown us the unit cell for the compound having $w = 0.499$ has even the larger volume than we could have seen previously for the similar *w* parameters. The main difference is in that the *c*-parameter is smaller in comparison to others and the *a*-parameter achieves almost the highest value: 3.9735 Å. The volume of unit-cell is then 122.305 Å^3.

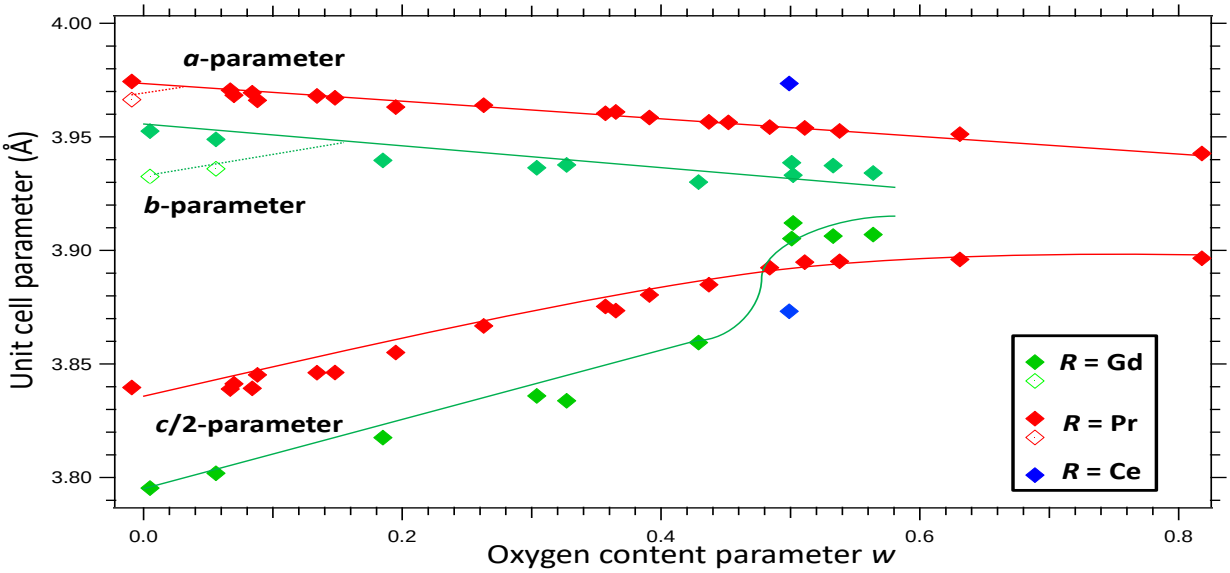

Figure 7 The unit-cell parameter evolution for RBaFe$_2$O$_{5+w}$ with R = Gd, Ba and Ce

Conclusions

In the Figure 8, the oxygen content parameter w evolution over all investigated rare-earth elements is given.

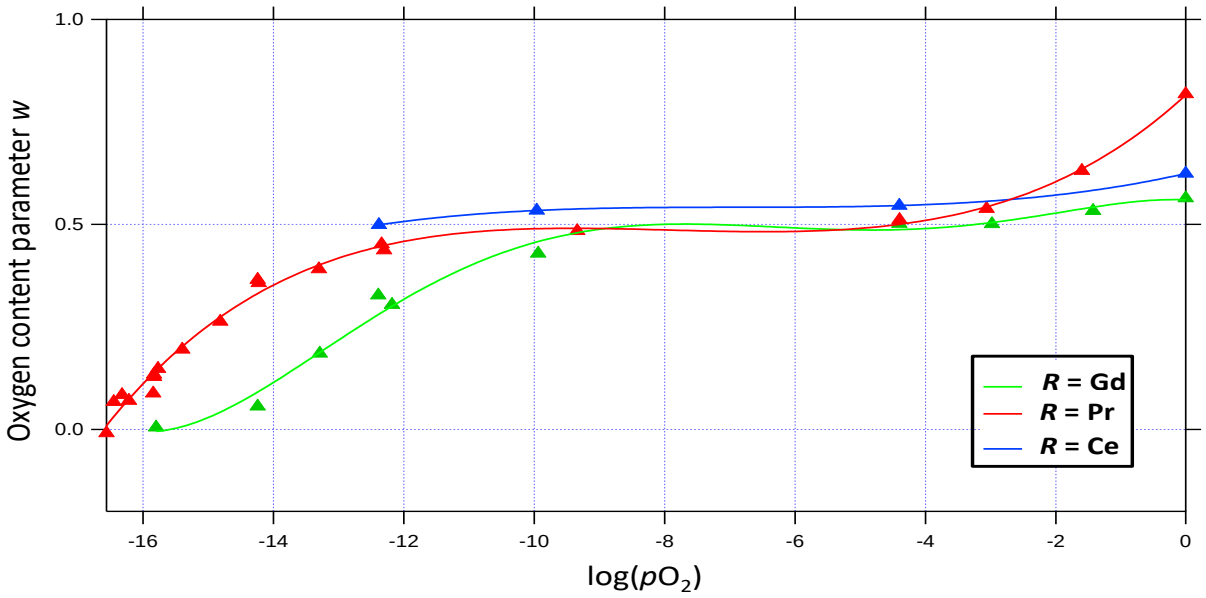

Figure 8 Summary of the oxygen content parameter *w* over the log(pO_2) for all *R* = Gd, Pr and Ce

Based on the given comparison and also on the evaluation of the unit-cell parameters (Figure 7) we can state the following conclusions:

- For $GdBaFe_2O_{5+w}$ and $PrBaFe_2O_{5+w}$ we observed the wide nonstoichiometry range, the wider for *R* = Pr within the interval $-0.009 \leq w \leq 0.818$. It says us each of those synthesized double-cell perovskite phases is very stable and available to contain various portion of oxygen atoms into its structure

- For *R* = Gd and Pr, we didn't observed the oxidative decomposition even in the atmosphere of pure O_2; the maximal limits of *w* are achievable. For *R* = Ce, partly decomposed non-magnetic product was observed after the equilibration in the lowest used partial pressure of oxygen

- We observed the huge difference in the highest achievable values of *w* in pure O_2 for $GdBaFe_2O_{5.564}$ and $PrBaFe_2O_{5.818}$. This is caused by the different atomic radius of *R*. The smallest Gd atoms (*r* = 1.053 Å [15]) cause the denser structure also with the less available space for the oxygen accommodation. The larger Pr (*r* = 1.126 Å [16]) provides more flexible environment having also the larger unit-cell and allows the higher accommodation of oxygen into the structure. In case of Ce (*r* = 1.143 Å [17]), we would expect even the higher achievable oxygen parameter *w*. However, we observed the

smaller limits in the section of oxygen content analysis, most probably because of the sample decomposition and some solid oxides formation. This needs to be further investigated, the products of decomposition need to be determined and the reasons of decomposition should be identified

- During the oxygen loading into the structure, the expansion mainly in one dimension is observed, while the contraction in another occurs upon the increasing amount of oxygen: the *c*-parameter of the unit-cell increases, whereas the *a*-parameter lowers. Also the *b*-parameter closers to the *a*-parameter. This causes the transition between orthorhombic (for lower *w*) and tetragonal (for higher *w*) crystal system.

- A trend was observed: while the oxygen content parameter *w* got close to the value 0.5 (for Gd and Pr), the phase always gained a big increase in its volume. The volume decrease was observed with any small variation either above or below the value 0.5 The reasons for this need to be further investigated, based on the consideration of processes happening while the w = 0.5

The highest achievable limits of *w* in $R\mathrm{BaFe_2O_{5+w}}$ when *R* = Gd and Pr were successfully observed. The detailed study of the *w* parameter variation when *R* = Pr was provided, as well as the overview for *R* = Gd was performed. The unit cell parameter investigation was done for the main part of the obtained samples. Also the unit-cell parameter evolution was described in the study. In case of *R* = Ce, some problems with the phase purity occurred after the equilibration and needs to be further investigated.

---

[1] P. Karen, P. Woodward, *Synthesis and structural investigations of the double perovskites $REBaFe_2O_{5+w}$ (RE = Nd, Sm)*, J. Mater. Chem. 9(1999)789–797.

[2] J. Lindén, P. Karen, A. Kjekshus, J. Miettinen, T. Pietari, M. Karppinen, *Valence-state mixing and spearation in $SmBaFe_2O_{5+w}$*, Physical Review B 60(1999) 251-260.

[3] P. Karen, P. Woodward, J. Linden, T. Vogt, A. Studer, P. Fischer, *Verwey transition in mixed-valence $TbBaFe_2O_5$*, Physical review B 64(2001)214405.

[4] J. Nakamura, M. Kaeppinen, P. Karen, J. Lindén, H. Yamauchi, *Isovalent-substitution effect on the Verwey-type transition in the A-site-ordered double perovskite (Ba, Sr)RFe_2O_5*, Physical review B 70(2004)144104.

[5] J. Lindén, P. Karen, J. Nakamura, M. Karppinen, H. Yamauchi, *Transport and magnetotransport properties across the two-step Verwey transition in $BaGdFe_2O_{5+w}$*, Physical review B 73(2006)064415.

[6] P. Karen, P. Woodward, P. Santhosh, T. Vogt, P. Stephens, S. Pagola, *Verwey Transition under Oxygen Loading in $RBaFe_2O_{5+w}$ (R = Nd and Sm)*, Journal of Solid State Chemistry 167(2002)480-493.

[7] P. Karen, *Effects of oxygen nonstoichiometry and of its distribution on Verwey-type transitions and structure of $GdBaFe_2O_{5+w'}$*, Journal of Solid State Chemistry 170(2003)9–23.

[8] P. Woodward, E. Suard, P. Karen, *Structural Tuning of Charge, Orbital, and Spin Ordering in Double-Cell Perovskite Series between $NdBaFe_2O_5$ and $HoBaFe_2O_5$*, J. Am. CHem. Soc. 125(2003)8889-8899.

[9] P. Woodward, P. Karen, *Mixed Valence in $YBaFe_2O_5$*, Inorganic Chemistry 42(2003)1121-1129.

[10] P. Karen, *Chemistry and thermodynamics of the twin charge/ordering transitions in $RBaFe_2O_{5+w}$ series*, Solid State Chemistry 177(2004) 281-292.

[11] A. C. Larson, R. B. Von Dreele, *General Structure Analysis System (GSAS)*, Los Alamos National Laboratory Report LAUR(2000) 86-748.

[12] S. Ikeda, J.M. Carpenter, Nuc. Inst. And Meth., A239(1985)536-544.
[13] P. Thompson, D. E. Cox, J. B. Hastings, J. Appl. Cryst., 20(1987)79-83.
[14] P. Karen, unpublished.
[15] R. D. Shannon, *Revised effective ionic radii and systematic studies of interatomic distances in halides and chalcogenides*, Acta Cryst. 32 (1976) 751-767.
[16] R. D. Shannon, *Revised effective ionic radii and systematic studies of interatomic distances in halides and chalcogenides*, Acta Cryst. 32 (1976) 751-767.
[17] R. D. Shannon, *Revised effective ionic radii and systematic studies of interatomic distances in halides and chalcogenides*, Acta Cryst. 32 (1976) 751-767.